Heterogeneous subunit structures in the pyranose 2-oxidase homotetramer revealed by theoretical analysis of the rates of photoinduced electron transfer from a tryptophan to the exc...

ARTICLE *in* JOURNAL OF PHOTOCHEMISTRY AND PHOTOBIOLOGY A CHEMISTRY · MARCH 2015

Impact Factor: 2.5 · DOI: 10.1016/j.jphotochem.2015.03.016

8 AUTHORS, INCLUDING:

Kiattisak Lugsanangarm
Chulalongkorn University
17 PUBLICATIONS **82** CITATIONS
SEE PROFILE

Arthit Nueangaudom
Chulalongkorn University
13 PUBLICATIONS **40** CITATIONS
SEE PROFILE

Fumio Tanaka
Chulalongkorn University
112 PUBLICATIONS **1,134** CITATIONS
SEE PROFILE

Seiji Taniguchi
Institute for laser technology
77 PUBLICATIONS **2,216** CITATIONS
SEE PROFILE

Journal of Photochemistry and Photobiology A: Chemistry 306 (2015) 66–79

Contents lists available at ScienceDirect

Journal of Photochemistry and Photobiology A: Chemistry

journal homepage: www.elsevier.com/locate/jphotochem

Heterogeneous subunit structures in the pyranose 2-oxidase homotetramer revealed by theoretical analysis of the rates of photoinduced electron transfer from a tryptophan to the excited flavin

Kiattisak Lugsanangarm [a], Arthit Nueangaudom [a], Sirirat Kokpol [a], Somsak Pianwanit [a,*], Nadtanet Nunthaboot [b], Fumio Tanaka [a,c,**], Seiji Taniguchi [c], Haik Chosrowjan [c]

[a] Department of Chemistry, Faculty of Science, Chulalongkorn University, Bangkok 10330, Thailand
[b] Department of Chemistry, Faculty of Science, Mahasarakham University, Mahasarakham 44150, Thailand
[c] Division of Laser BioScience, Institute for Laser Technology, Utsubo-Honmachi, 1-8-4, Nishiku, Osaka 550-0004, Japan

ARTICLE INFO

Article history:
Received 25 December 2014
Received in revised form 15 March 2015
Accepted 19 March 2015
Available online 20 March 2015

Keywords:
Pyranose 2-oxidase
Molecular dynamics simulation
Photoinduced electron transfer

ABSTRACT

Pyranose 2-oxidase (P2O) from *Trametes multicolor* forms a homotetramer in which each of the subunits contains flavin adenine dinucleotide (FAD). The fluorescence of P2O decays with two lifetime components; a slow (358 ps) and a fast (~90 fs) decay. The lifetime of the fast component is emission-wavelength dependent and is ascribed to fast photoinduced electron transfer (ET) from Trp168 to the excited isoalloxazine (Iso*) in FAD. The donor–acceptor distances were ~0.7 nm. The extraordinary heterogeneous decays were analyzed with atomic coordinates obtained by a molecular dynamics simulation and the ET rate by Kakitani and Mataga. The emission-wavelength dependent decays in the fast component were elucidated by introducing emission-wavelength dependent standard free energy related to electron affinity of Iso*. Examination of all possible combinations of the four subunits revealed that the slow component was from subunit A and the fast component was from the other three subunits. Agreements between the observed and calculated decays were all excellent. The large difference in the fast and slow fluorescent lifetimes is ascribed to the difference in the standard free energy gap related to electron affinity of Iso*. The dependence of the logarithmic ET rates on the center-to-center distance displayed approximate linear functions (Dutton rule) when the rate was relatively slow and parabolic functions when the rate was ultrafast. The Dutton rule originated from the exponential term of the ET rate, not from the electronic coupling term.

1. Introduction

Pyranose 2-oxidase from *Trametes multicolor* (P2O) forms a homotetramer in which each subunit contains flavin adenine dinucleotide (FAD) as a coenzyme with a molecular weight (Mw) of 68 kDa [1]. In nature, P2O is distributed in the hyphal periplasmic space of wood-degrading basidiomycetes, [2] and catalyzes oxidative degradation of lignin to produce hydrogen peroxide (H_2O_2) [3]. Each FAD is covalently linked to the respective P2O subunit His167 residue via the flavin 8α-methyl group [4]. Several crystal structures of P2O have been determined, [5–7] and the reaction mechanisms of P2O have been investigated by transient kinetics, kinetic isotope effects and site-directed mutagenesis [8–11].

It was recently demonstrated that the ultrafast fluorescence dynamics of P2O displays two transient fluorescence spectra with different lifetimes of a mean of 88 fs and 358 ps in the wild type (WT) P2O [12]. The shorter lifetime fluorescence displayed a time-dependent spectra with a peak emission at ca. 540 nm, while the longer lifetime displayed a time-independent spectrum at ca. 510 nm. The ultrashort lifetimes were ascribed to the photoinduced electron transfer (ET) from Trp168 to the excited isoalloxazine (Iso*) [12]. The long lifetime emission peak was similar to that obtained by steady-state excitation, suggesting that the fluorescence spectrum under steady-state excitation is likely to be derived from the same source as the long lifetime fluorescence. The characteristics of the transient behaviour of the fluorescence from the WT P2O are similar to the H167A and T169S single substitution isoforms of P2O with and without an acetate ligand [13]. The conformational heterogeneities in the WT and point mutated P2Os

* Corresponding author. Tel.: +66 22187602.
** Corresponding author at: Division of Laser BioScience, Institute for Laser Technology, Utsubo-Honmachi, 1-8-4, Nishiku, Osaka 550-0004, Japan.
E-mail addresses: somsak.t@chula.ac.th (S. Pianwanit), fumio.tanaka@yahoo.com (F. Tanaka).

http://dx.doi.org/10.1016/j.jphotochem.2015.03.016
1010-6030/

were previously elucidated using the ET parameters contained in a theoretical ET rate given by Kakitani and Mataga (KM) theory, [14–17] and using the atomic coordinates with crystal structures [5–7]. The geometrical factors, such as the donor–acceptor distance and the H-bond distances, however, were found to be almost identical among the four subunits in the crystal structures. Hence, the heterogeneous conformations of P2O were elucidated in terms of the static dielectric constant of the entire protein.

It is very important to clarify whether the geometrical factors that are influential upon the ET rate are really uniform among the four subunits in solution. Structural heterogeneity among the four subunits of P2O was theoretically demonstrated in solution by molecular dynamics simulation (MDS) [18]. In the present work the experimental fluorescence dynamics of P2O were analyzed with MDS atomic coordinates and KM ET rate, and demonstrated subunit-based heterogeneity of the ET rates in the WT P2O.

2. Method of analyses

2.1. Molecular dynamics simulation

Details of MDS calculation were described in the previous work [18]. The initial WT P2O structure (pdb code: 2IGK) was retrieved from the Protein Data Bank [Research Collaboratory for Structural Bioinformatics (RCSB)]. Subsequently, all missing atoms were added using the Discovery Studio 2.0 software (Website, www.accelrys.com). Then, all missing hydrogen atoms were added using the LEaP module of the Amber version 10 suite package [19].

The force field parameters of FAD were taken from previous work [20]. The MD simulation was performed by using Amber10 and the amber03 force field was employed [19]. The geometrical crash of hydrogen atoms were removed by minimizing with 2000 steps of the steepest decent (SD) algorithm, followed by 3000 steps of conjugate gradient (CG) algorithm. The TIP3P water model was used as solvent. P2O protein was solvated by 63000 TIP3P water molecules, extending at the distance of 10 Å in each of the six directions: ($\pm x$, $\pm y$, and $\pm z$) around the P2O protein, result in the cubic box with the length of $147 \times 129 \times 140$ Å. Subsequently, appropriate counter ions were added into the simulation box to neutralize the charged residues. The secondary minimization of the whole system (protein, solvent and counter ion) was carried out with 2000 steps of SD and 3000 steps of CG minimization, respectively. The MD simulation was controlled under constant temperature and pressure ensemble (*NPT*) with a constant pressure of 1 atm and constant temperature of 298 K. The Berendsen thermostat was applied to control the temperature and the SHAKE algorithm [21] was employed to constrain all bonds involving hydrogen atoms throughout MD simulation. The long-range electrostatic interaction was described by a particle mesh Ewald approach with a spherical cutoff of 10.0 Å [22]. The MD simulations were calculated for 20 ns with a 0.002 ps time interval. The equilibration of the whole MD simulations system was observed by the global root of mean square deviation (RMSD). The MD simulations coordinates were collected from 15 ns to 20 ns of the production time with a time interval of 0.2 ps. A total of 25000 snapshots were used for the present analysis.

2.2. ET rate

The original Marcus theory [23,24] has been modified in various ways [14–17,25]. In the present analysis, KM theory [14–17] was used because it is applicable for both non-adiabatic and adiabatic ET processes, and has been found to give satisfactory results for both static ET analysis with fluorescence lifetimes [13,26–28] and dynamic ET analyses with fluorescence decays of flavoproteins [29–33]. The observed fluorescence decays in P2O were non-exponential, and expressed as two-exponential decay functions [12]. The fast component, with a lifetime of ~88 fs was emission-wavelength (λ) dependent, while the slow component, with a lifetime of 358 ps, was emission-wavelength independent. The emission-wavelength dependent ET rates for the fast component described by the KM model for P2O were expressed by Eq. (1).

$$k_{ij}^{f} = \frac{\nu_0^f}{1+\exp\left\{\beta^f\left(R_i - R_0^f\right)\right\}}\sqrt{\frac{k_B T}{4\pi\lambda_S^{if}}}\exp \left[-\frac{\left\{\Delta G_{fj}^0 - e^2/\varepsilon_{DA}^f R_i + \lambda_S^{if} + E_{Net}^{if}\right\}^2}{4\lambda_S^{if} k_B T}\right] \quad (1)$$

The P2O monomer contains 9 tryptophan (Trp) and 15 tyrosine (Tyr) residues. In the present work the ET rates only from Trp168 were taken into account among these aromatic amino acids, because the Trp168–Iso distance is within 0.8 nm in all subunits, while those in the other aromatic amino acids were longer than 1.2 nm (Table S1, Supporting information (SI)) [12]. In Eq. (1),k_{ij}^f is the ET rate of the fast component from Trp168 to the Iso* in subunit i at the emission wavelength j, ν_0^f is an adiabatic frequency and β^f is the ET process coefficient of the fast component. R_i and R_0^f are the Trp168–Iso distances in subunit i and its critical distance for the ET process of the fast component, respectively. Note that R_i is expressed as a center-to-center distance (R_c) rather than as an edge-to-edge (R_e) distance [13,26–33]. The ET process is adiabatic when $R_i \le R_0^f$, and non-adiabatic when $R_i > R_0^f$. The term $-e^2/\varepsilon_{DA}^f R_i$ in Eq. (1) is the electrostatic energy (ES) between the Iso anion and a donor cation (ESDA), where ε_{DA}^f is the static dielectric constant between Trp168 and Iso in the fast component. The terms k_B, T, and e are the Boltzmann constant, temperature and electron charge, respectively. E_{Net}^{if} is the net ES energy (Net*ES*) of Trp168 in subunit i for the fast component, which is described later. λ_S^{if} is the solvent reorganization energy [23,24] of the ET donor in subunit i for the fast component, and is expressed in Eq. (2).

$$\lambda_S^{if} = e^2\left(\frac{1}{2a_{Iso}} + \frac{1}{2a_{Trp}} - \frac{1}{R_i}\right)\left(\frac{1}{\varepsilon_\infty} - \frac{1}{\varepsilon_{DA}^f}\right), \quad (2)$$

where a_{Iso} and a_{Trp} are the radii of Iso and Trp and ε_∞ is optical dielectric constant. In this study the previously determined [13,26–33] values of Iso (a_{Iso}) and Trp (a_{Trp}) of 0.224 and 0.196 nm, respectively, were used, which assumes that they are spherical, whilst ε_∞ was set at 2.0.

The standard free energy gap for the fast component was expressed with the ionization potential of Trp (E_{IP}) by Eq. (3).

$$\Delta G_{fj}^0 = E_{IP} - G_{fj}^0 \quad (3)$$

Here G_{fj}^0 is the standard Gibbs energy related to the electron affinity of Iso* of the fast component at an emission wavelength j. The experimental value of E_{IP} for Trp is 7.2 eV [34]. It was assumed that the ET rate of the fast component was emission-wavelength dependent through G_{fj}^0, because G_{fj}^0 is related to the electronic energy of Iso*, and further it depends on hydrogen bonds (H-bonds) between Iso* and the surrounding amino acids [27,28].

Table 1
Chi-square values for all possible combinations of the fast and slow fluorescence components among the four subunits of P2O.[a]

Case (n)	Subunit				$\chi_T^2(n)$
	Sub A	Sub B	Sub C	Sub D	
1	Slow	Fast	Fast	Fast	2.63×10^{-5}
2	Fast	Slow	Fast	Fast	6.50×10^{-1}
3	Fast	Fast	Slow	Fast	3.55×10^{-4}
4	Fast	Fast	Fast	Slow	3.47×10^{-4}
5	Fast	Slow	Slow	Slow	5.83×10^{-1}
6	Slow	Fast	Slow	Slow	3.42×10^{-1}
7	Slow	Slow	Fast	Slow	3.34×10^{-2}
8	Slow	Slow	Slow	Fast	4.02×10^{-1}
9	Slow	Slow	Fast	Fast	3.33×10^{-2}
10	Slow	Fast	Slow	Fast	6.79×10^{-1}
11	Slow	Fast	Fast	Slow	6.82×10^{-1}
12	Fast	Slow	Slow	Fast	3.33×10^{-2}
13	Fast	Slow	Fast	Slow	3.33×10^{-2}
14	Fast	Fast	Slow	Slow	3.37×10^{-2}

[a] Chi-square values ($\chi_T^2(n)$) were evaluated for all possible combinations of $F^f_{calc}(t\lambda_j)$ and $F^s_{calc}(t)$ (Eqs. (11) and (12)). $\chi_T^2(n)$ was expressed by Eq. (13). The value of $\chi_T^2(n)$ was smallest when Sub A was the slow fluorescence component and Sub B, Sub C and Sub D were the fast subunits ($n = 1$).

The ET rate for the slow component was expressed by Eq. (4).

$$k_i^s = \frac{\nu_0^s}{1+\exp\{\beta^s(R_i - R_0^s)\}}\sqrt{\frac{k_BT}{4\pi\lambda_S^{is}}}\exp\left[-\frac{\left\{\Delta G_s^0 - e^2/\varepsilon_{DA}^s R_i + \lambda_S^{is} + E_{Net}^{is}\right\}^2}{4\lambda_S^{is}k_BT}\right], \quad (4)$$

where ν_0^s is an adiabatic frequency, β^s the ET process coefficient, R_0^s the critical distance for the slow component and λ_S^{is} is the solvent reorganization energy for the slow component, given by Eq. (5).

$$\lambda_S^{is} = e^2\left(\frac{1}{2a_{Iso}} + \frac{1}{2a_{Trp}} - \frac{1}{R_i}\right)\left(\frac{1}{\varepsilon_\infty} - \frac{1}{\varepsilon_{DA}^s}\right), \quad (5)$$

where ΔG_s^0 is the standard free energy gap of the slow component between the products and reactants, and is expressed by Eq. (6).

$$\Delta G_s^0 = E_{IP} - G_s^0 \quad (6)$$

Here G_s^0 is the free energy of Iso* of the slow component. The other variables and constants in Eq. (4) are as per Eq. (1).

2.3. ES of the P2O tetramer

Protein systems contain many ionic groups, which may influence the ET rate. The FAD cofactor in P2O has two negative charges at the pyrophosphate, whilst P2O itself contains 34 glutamine (Glu), 37 aspartate (Asp), 26 lysine (Lys) and 27 arginine (Arg) residues per subunit. Therefore, the total numbers of ionic groups are four times of those in one subunit. The ES energy between the Iso anion or Trp168 cation and all other ionic groups in subunit i (Sub A–Sub D) of the component c is expressed by Eq. (7).

$$E_j^{ci} = \sum_{l=1}^{4}\sum_{k=1}^{34}\frac{C_j \cdot C_{Glu}}{\varepsilon_0^c R_{li}(\mathrm{Glu}-k)} + \sum_{l}^{4}\sum_{k=1}^{37}\frac{C_j \cdot C_{Asp}}{\varepsilon_0^c R_{li}(\mathrm{Asp}-k)} + \sum_{l=1}^{4}\sum_{k=1}^{26}\frac{C_j \cdot C_{Lys}}{\varepsilon_0^c R_{li}(\mathrm{Lys}-k)} + \sum_{l=1}^{4}\sum_{k=1}^{27}\frac{C_j \cdot C_{Arg}}{\varepsilon_0^c R_{li}(\mathrm{Arg}-k)} + \sum_{l=1}^{4}\sum_{k=1}^{4}\frac{C_j \cdot C_P}{\varepsilon_0^c R_{li}(P-k)} \quad (7)$$

Here $j = 0$ for the Iso anion in subunit i, 1 for the Trp168 cations. The component c is f for the fast component and s for the slow component. C_j is the charge of the aromatic ionic species j, that is $-e$ for $j = 0$ and $+e$ for $j = 1$. The terms C_{Glu} (=$-e$), C_{Asp} (=$-e$), C_{Lys} (=$+e$) and C_{Arg} (=$+e$) are the charges of the Glu–Asp–Lys and Arg residues, respectively. FAD contains two phosphate atoms, each of which binds two oxygen atoms. It was assumed that the charge of each oxygen atom is EC = $-0.5e$, although the total charge of four oxygen atoms is $-2e$. We also assumed that these groups are all in an ionic state in solution at pH 7.0 since the pK_a values of these amino acids in water are 4.3 (Glu), 3.9 (Asp), 10.5 (Lys) and 12.5 (Arg). Histidine (His) has a pK_a of 6.0 in water and varies from 5.5 to 6.7 in the protein (RNase A) [35–37]. Since all the measurements were performed at pH 7.0, the His residues should be deprotonated and neutral. The distances between the aromatic ionic species j and the kth Glu ($k = 1$–44) are denoted as EC, whilst the distances between the aromatic ionic species j and the kth Asp ($k = 1$–37) are denoted as EC, and so on for other ionic amino acid residues. EC is the static dielectric constant of component c.E_{Net}^{ic} in Eq. (1) was then expressed as Eq. (8).

$$E_{Net}^{ic} = E_0^{ic} + E_1^{ic} \quad (8)$$

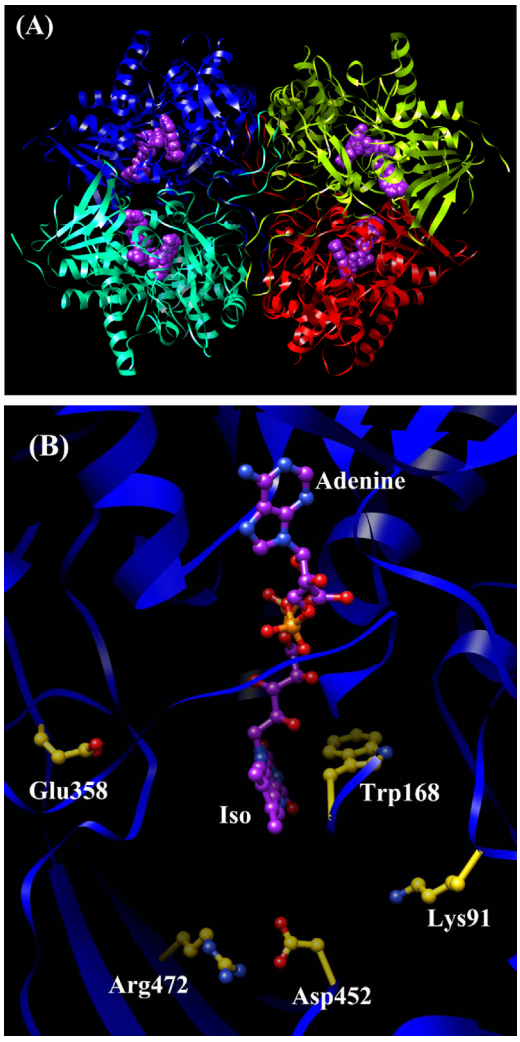

Fig. 1. The three-dimensional structure of P2O.
(A) The structure of the whole tetrameric protein, with blue for subunit-A, green for subunit-B, yellow for subunit-C and red for subunit-D, respectively. The FAD molecules in the tetramer are indicated with magenta stick models. (B) The FAD binding site including Trp168 and the other local ionic amino acids.

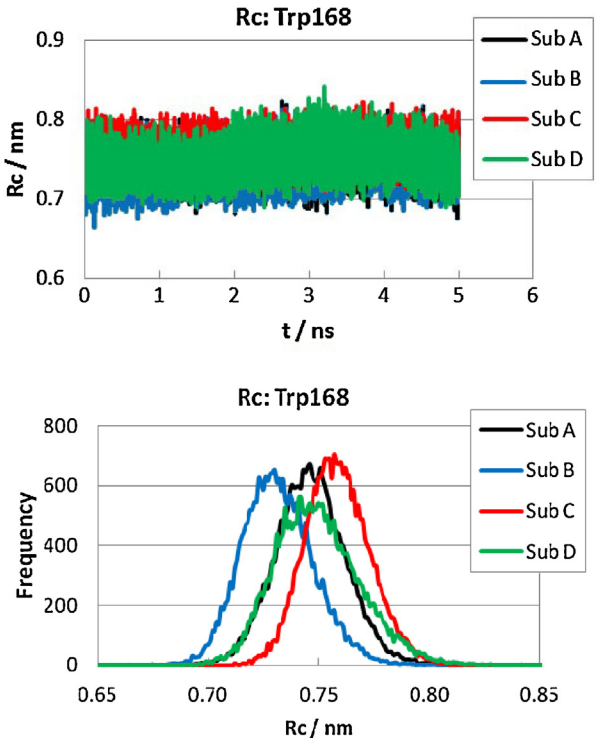

Fig. 2. The (upper panel) dynamics and (lower panel) distribution of the R_c between Iso and Trp168. Trp168 is the shortest distance to Iso among the aromatic amino acids. Inserts denote four subunits.

2.4. Experimental fluorescence decays of WT P2O

The observed decay functions for the fast and the slow fluorescent components are expressed by Eqs. (9) and (10), respectively.

$$F_f(t\lambda_j) = \exp(\frac{-t}{\tau_j^f}) \tag{9}$$

$$F_s(t) = \exp(\frac{-t}{\tau^s}) \tag{10}$$

The observed decay parameters are listed in Table S2 (SI) [12]. In Eq. (9) $\lambda_1 = 580$ nm and $\tau_1^f = 0.092$ ps, $\lambda_2 = 555$ nm and $\tau_2^f = 0.113$ ps, $\lambda_3 = 530$ nm and $\tau_3^f = 0.110$ ps, $\lambda_4 = 500$ nm and $\tau_4^f = 0.070$ ps, $\lambda_5 = 480$ nm and $\tau_5^f = 0.057$ ps (mean 88 fs). The decay for the slow component is emission-wavelength independent. The value of the lifetime is $\tau^s = 358$ ps.

2.5. Calculated fluorescence decay functions

The calculated decay functions of the fast and slow fluorescence components are expressed by Eqs. (11) and (12), respectively.

$$F_{\text{calc}}^f(t\lambda_j) = \frac{1}{m}\sum_{i=1}^{m}\left\langle \exp\left[-\left\{k_{ij}^f(t')\right\}t\right]\right\rangle_{\text{AV}} (\text{j} = 1-5) \tag{11}$$

$$F_{\text{calc}}^s(t) = \frac{1}{4-m}\sum_{i=1}^{4-m}\langle \exp\left[-\{k_i^s(t')\}t\right]\rangle_{\text{AV}} \tag{12}$$

where $k_{ij}^f(t')$ and $k_i^s(t')$ are MDS time (t')-dependent because the donor–acceptor distances and E_{Net}^i depend on t', although the ET rates given by Eqs. (1) and (4) are time-independent. $F_{\text{calc}}^f(t\lambda_j)$ in Eq. (10) depends on the emission-wavelength λ_j ($j = 1-5$). In the present model it was assumed that m subunits among the four subunits display fast decay, and 4-m subunits the slow decay. In Eq. (12) τ_i^f is the decay function of the slow component and is independent of the emission wavelength.

When $m = 1$, there should be four possible fast decays (each five decays with j), namely i = Sub A, Sub B, Sub C and Sub D. In the case that Sub A is the fast component, Sub B, Sub C and Sub D are the slow components. In the case that Sub B is the fast component, Sub A, Sub C and Sub D are the slow components, and likewise for when Sub C or Sub D are the fast component, the other three subunits are the slow components. When $m = 2$, there should be six combinations of τ^s and α_i^f. If Sub A and Sub B are fast components, then Sub C and Sub D should be slow components, and so on. When $m = 3$, there should be four possible combinations of α^s and τ_i^f, namely, Sub B, Sub C and Sub D are fast components (Sub A is a slow component). Accordingly there are altogether 14 sets of τ^s and α_i^f (Table 1).

The fluorescence decays were calculated up to 0.6 ps with 0.0012 ps time intervals for the fast decay and 500 ps with 1 ps time intervals for the slow decay. Note that α^s denotes the averaging procedure of the exponential functions in Eqs. (11) and (12) over the MDS time t'. The averaging procedures were performed up to 5 ns with 0.2 ps time intervals over 25000 snapshots [18].

2.6. Determination of the ET parameters

Initially the ET parameters related to the electronic coupling term ($\angle$, β^c and R_0^c) of Trp for both the fast and slow components ($c = f$ or s for the fast or slow component, respectively) were taken from the reported values in the flavin mononucleotide binding proteins (FBP) [30]. In this model the unknown ET parameters were G_{fj}^0 (λ_j; $j = 1$–5), G_s^0 (for the slow component; λ-independent), ε_0^c ($c = f$ and s) and $\chi_T^2(n)$ ($c = f$ and s). The fittings between the observed and calculated decays, however, were not satisfactory. Accordingly, $\chi_T^2(n)$, $F_{\text{calc}}^f(t\lambda_j)$ and $F_{\text{calc}}^s(t)$ ($c = f$ and s) for Trp were added as unknown parameters. Therefore, there were 16 unknown ET parameters altogether of: $\chi_T^2(n)$, $\chi_T^2(n)$ and λ_j ($c = f$ and s), G_{fj}^0 (G_s^0; $j = 1$–5), ΔG_{fj}^0, ΔG_s^0 ($c = f$ and s) and $\chi_{fn}^2(\lambda_j)$ ($c = f$ and s). These parameters were varied so as to obtain the minimum value of total chi-square, as expressed by Eqs. (13)–(15).

$$\chi_T^2(n) = \sum_{j=1}^{5}\chi_{fn}^2(\lambda_j) + \chi_{sn}^2 \tag{13}$$

$$\chi_{fn}^2(\lambda_j) = \frac{\{F_{\text{calc}}^f(t\lambda_j) - F_f(t\lambda_j)\}^2}{F_{\text{calc}}^f(t\lambda_j)} \tag{14}$$

$$\chi_{sn}^2 = \frac{\{F_{\text{calc}}^s(t) - F_s(t)\}^2}{F_{\text{calc}}^s(t)} \tag{15}$$

where $\chi_{fn}^2(\lambda_j)$ is the total chi-square of nth combination, as shown in Table 1, while χ_{sn}^2 and ν_0^f are the chi-squares of the fast component at an emission wavelength β^f and the slow component for nth combination of R_0^f and ν_0^s, respectively. ET rates and other physical quantities were calculated with the best-fit ET parameters.

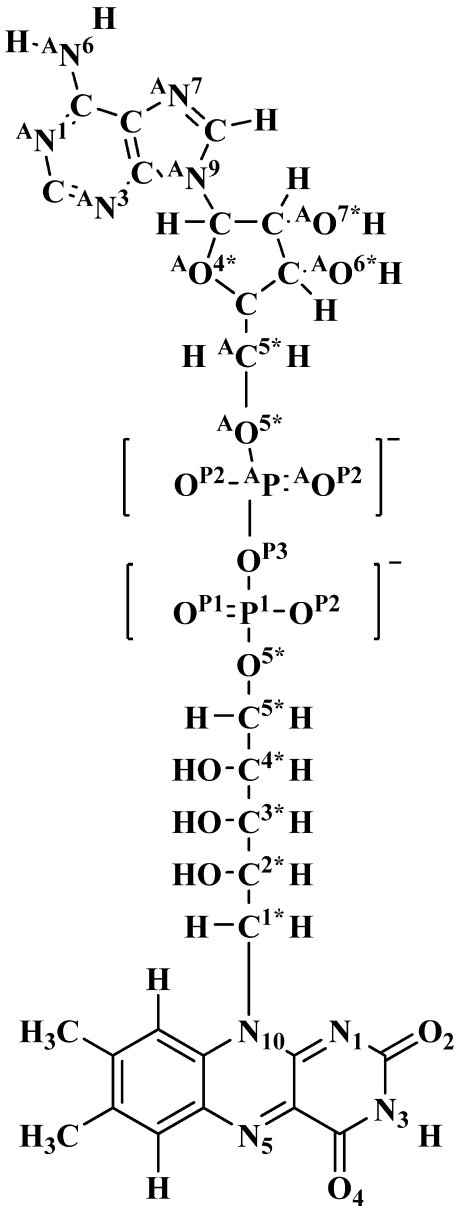

Chart 1. Chemical structure of FAD including the atomic numbering.

Deviations between the observed and calculated decays were evaluated using Eq. (16).

$$\text{Deviation}(t) = \frac{F_{\text{calc}(t)} - F_{\text{obs}}(t)}{\sqrt{F_{\text{calc}}(t)}}, \tag{16}$$

where R_0^s and ε_0^f represent the calculated and experimental decays, respectively.

3. Results

3.1. The donor–acceptor distance

The protein structure of P2O is shown in terms of the quaternary structure and the local structure around FAD in Sub A in Fig. 1, where Trp168 as a plausible ET donor and the ionic amino acids close to Iso are shown in addition to FAD. Fig. 2 shows the time-evolution of R_c between Iso and Trp168 (upper panel), and the R_c-distribution (lower panel) in all subunits. Seemingly, the R_c between Iso and several aromatic amino acids including Trp168 were not identical among the four subunits (Table S1, SI), and for Iso–Trp168 ranged from 0.73 nm (Sub B) to 0.76 nm (Sub C), whilst that for the other aromatic amino acids were all longer than 1.2 nm. However, in the crystal structure of P2O[6], the Iso–Trp168 R_c values (0.61 nm in Sub A, Sub C and Sub D, and 0.62 nm in Sub B) were almost identical amongst the four subunits but significantly shorter than the above MDS derived values. Regardless, in the present work only Trp168 was taken into account as the ET donor, because the R_c values between Iso and the other aromatic amino acids were much longer than that of Trp168 (>1.2 nm).

3.2. Hydrogen bonding between Iso and nearby amino acids

The H-bond distances (RHs) between Iso and the local amino acids are listed in Table S3 (SI), with the atom notations of Iso used (Chart 1) being taken from the PDB data. The N1 atom of Iso formed a H-bond with Thr553OG1 (side chain) in all subunits but with the shortest RH value in Sub D (0.30 nm) and the longest in Sub C (0.32 nm). The O2 atom of Iso formed H-bonds with Thr595N (peptide) and Thr595OG1 (side chain) with O2/Thr595N RH values of 0.30–0.31 nm. For the O2/Thr595OG1H-bond the RH value was shortest in Sub C (0.28 nm) and longest in Sub D (0.30 nm). The N3H of Iso formed a H-bond with Ala171O (peptide), in which the RH values were almost identical in all four subunits (0.285 nm). The O4 formed H-bonds with Cys170N (peptide), except in Sub B, and with the Ala171N (peptide), with almost identical RH values in the three subunits, and O4/Ala171N RH values of 0.30–0.31 nm. Finally, the N5 of Iso formed a relatively weak H-bond with Thr169 N (peptide) with RH values of 0.32–0.33 nm among the four subunits.

3.3. The observed and calculated fluorescence decays of P2O

The experimentally observed decay parameters, taken from the reported work, [12] are listed in Table S2 (SI), where the shorter lifetime fluorescence depends on the emission wavelength and the longer lifetime one does not. The observed and MDS calculated decay functions and their deviation from each other are shown in Fig. 3. The values of $\chi_T^2(n)$ were evaluated for all possible combinations of $F_{\text{calc}}^f(t\lambda_j)$ and $F_{\text{calc}(t)}^s$, derived from Eq. (13), are listed in Table 1. The $\chi_T^2(n)$ value was smallest when Sub A was the slow component and Sub B, Sub C and Sub D were the fast components ($n = 1$, $\chi_T^2(n) = 2.63 \times 10^{-5}$). The extent of coincidence of the calculated and observed decays was evaluated in terms of their deviation using Eq. (16) (Fig. 3) and the chi-square value (Table 2), and were found to be very small for all decays. This suggests that the present identification of the slow component as Sub A and the fast component as Sub B, Sub C and Sub D is reasonable.

3.4. Best-fit ET parameters

The emission-wavelength dependent best-fit ET parameters are listed in Table 2. The values of G_{fi}^0 for the fast component at different wavelengths, as derived from Eq. (3), ranged from 8.53 eV at 555 nm to 8.89 eV at 480 nm, which were all higher than that for the slow component ($G_s^0 = 7.33$ eV). The values of ΔG_{fi}^0 and ΔG_s^0, as obtained from Eqs. (3) and (6), respectively, and also listed in Table 2.

For the emission wavelength-independent ET parameters, the ν_0^f and ν_0^svalues (535 and 959 ps^{-1}, respectively) compared reasonably well with those of FBP (1016 ps^{-1}) [30] and the FD from *Helicobactor pylori* (1020 ps^{-1}) [33]. The frequency factor was about two-fold larger in the slow component compared to the fast

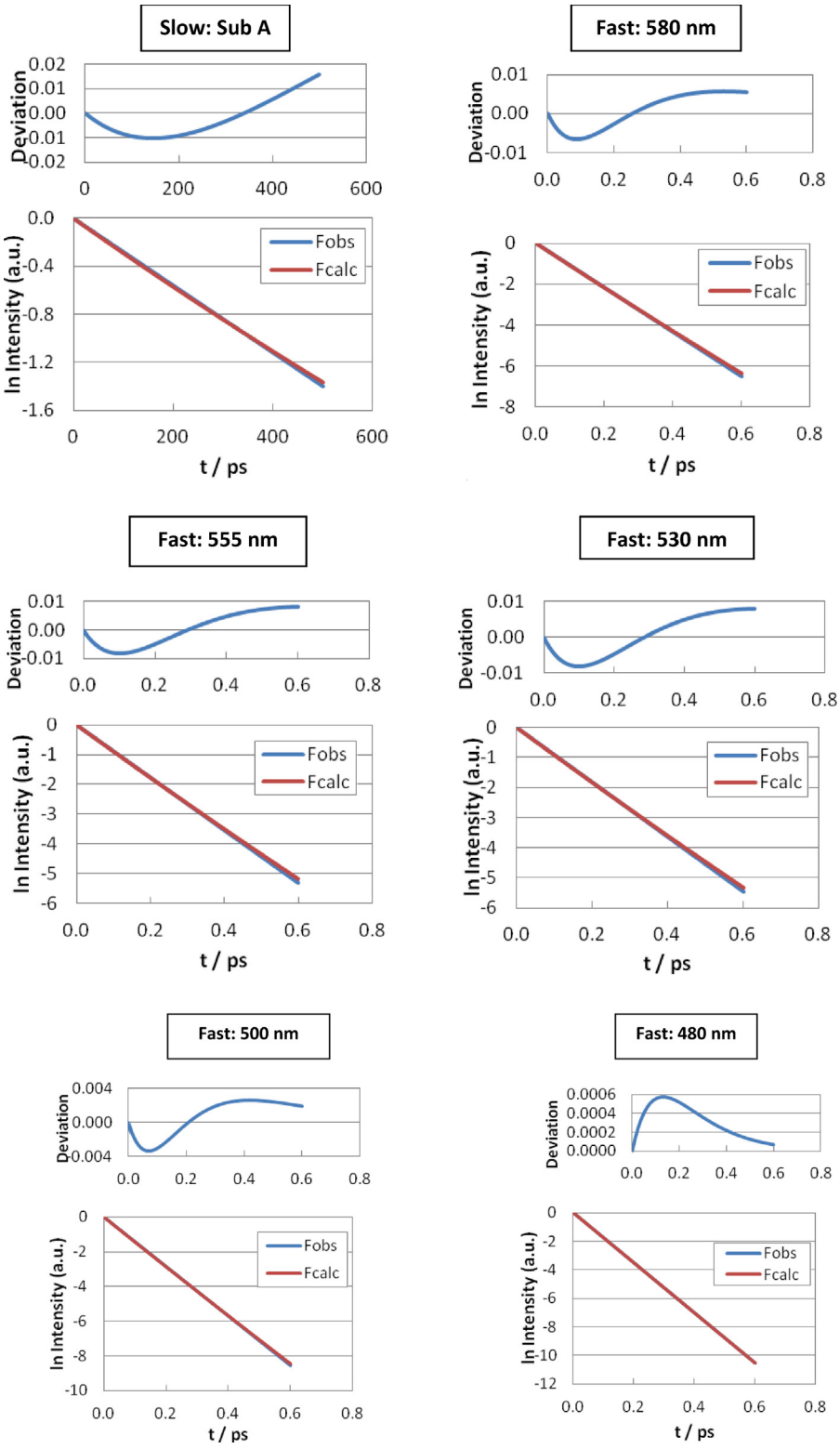

Fig. 3. The (lower panel) observed and calculated fluorescence decays of P2O and (upper panel) their deviation from each other.
Title of each panel denotes the emission-wavelength. Fobs and Fcalc in the inserts indicate the experimental and calculated fluorescence decays, respectively. Fcalc for the slow subunit was derived from Eq. (12) with $m = 1$ and i = Sub A, whilst for the fast subunits it was derived from Eq. (11) with $m = 1$, i = Sub B, Sub C and Sub D, and j = 580 nm, 555 nm, 530 nm, 500 nm and 480 nm, respectively.

component, despite the fact that the ET rates of the fast component were ~4000-fold greater than that of the slow component. The potential reasons for this are discussed later. The values of β^f and β^s were similar to each other (21.0 and 20.8 nm^{-1}, respectively) and to those of FBP [30] and FDs [33]. However, the values of R_0^f and R_0^s (1.3 and 1.2 nm, respectively) were much longer than those of FBP

Table 2
Determined standard free energy of Iso*.[a]

Fluorescent component	λ_j (nm)	G^0_{fj} (G^0_s) (eV)	ΔG^0_{fj} (ΔG^0_s) (eV)	$\chi^2_{fn}(\lambda_j)$ (χ^2_{sn})
Fast	580	8.59	−1.39	2.14×10^{-5}
	555	8.53	−1.33	3.45×10^{-5}
	530	8.54	−1.34	3.30×10^{-5}
	500	8.70	−1.50	4.88×10^{-6}
	480	8.89	−1.69	1.32×10^{-7}
Slow	530	(7.33)	(−0.13)	(6.36×10^{-5})

[a] The total chi-square value was 2.63×10^{-5} ($n = 1$). ΔG^0_{fj} and ΔG^0_s were obtained by Eqs. (3) and (6), respectively, and $\chi^2_{fn}(\lambda_j)$ and χ^2_{sn} were given by Eqs. (14) and (15), respectively.

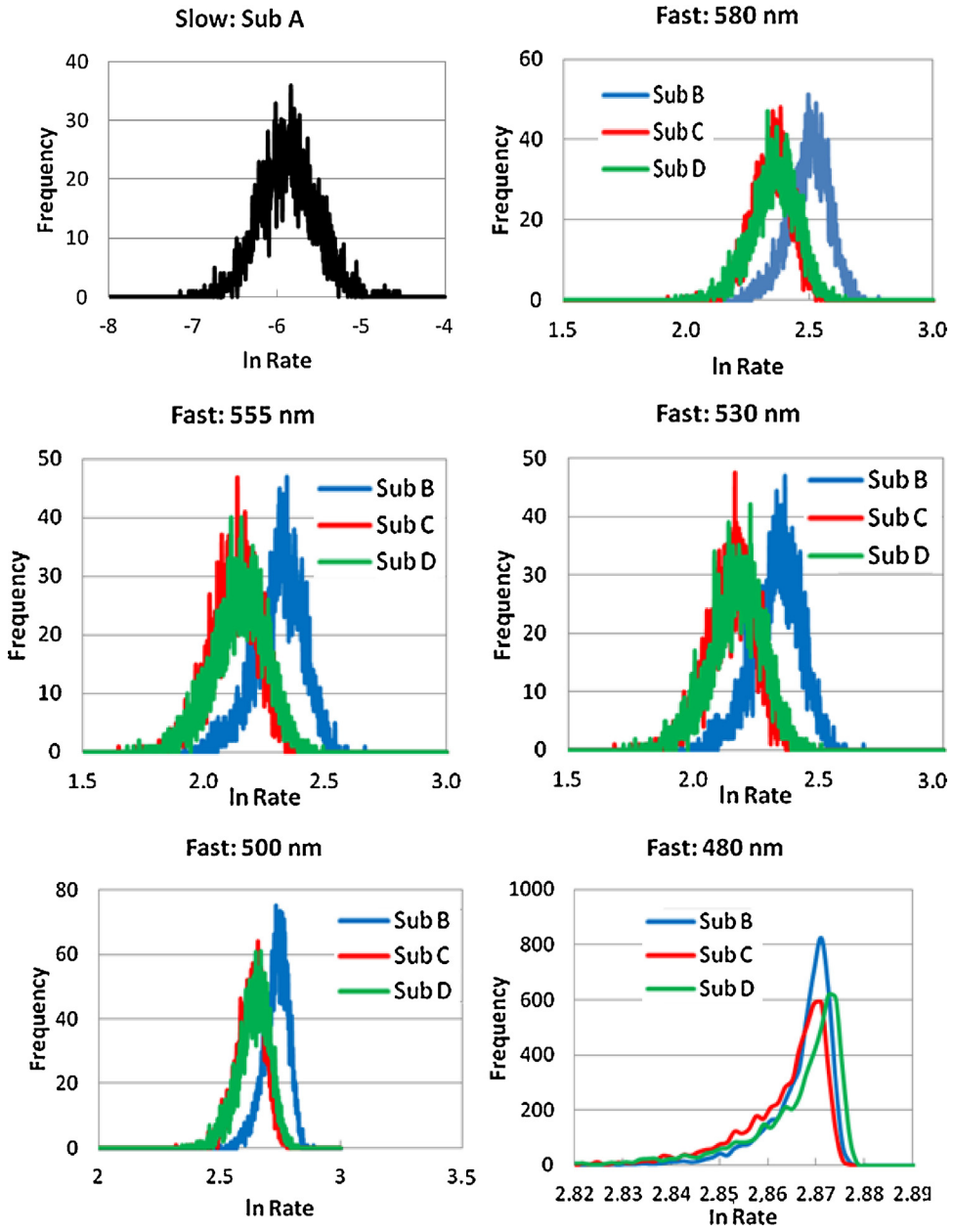

Fig. 4. Distribution of the logarithmic ET rate from Trp168 to Iso* in the P2O tetramer.
The rates of the fast components (Sub B, Sub C and Sub D) were emission-wavelength dependent,12, while the rate in the slow subunit (Sub A) was emission-wavelength independent. Rates are expressed in ps^{-1}.

Table 3
Physical quantity dependent on the emission wavelength.[a]

Component	Wavelength (nm)	Subunit	GT[b] (eV)	GTRAM[c]	Rate[d] (ps^{-1})	ln Rate
Fast	580 nm	Sub B	0.266	−0.381	12.1	2.50
		Sub C	0.315	−0.526	10.4	2.35
		Sub D	0.311	−0.514	10.6	2.36
	555 nm	Sub B	0.324	−0.566	10.1	2.31
		Sub C	0.374	−0.739	8.44	2.13
		Sub D	0.000	−0.726	8.59	2.15
	530 nm	Sub B	0.317	-0.541	10.4	2.34
		Sub C	0.367	−0.711	8.68	2.16
		Sub D	0.362	−0.698	8.83	2.18
	500 nm	Sub B	0.163	−0.145	15.3	2.73
		Sub C	0.212	−0.240	13.9	2.63
		Sub D	0.208	−0.232	14.0	2.64
	480 nm	Sub B	-0.0294	−0.00880	17.6	2.87
		Sub C	0.0201	−0.00561	17.5	2.86
		Sub D	0.0157	−0.00551	17.5	2.86
Slow		Sub A	1.24	−9.40	0.00296	-5.82

[a] Mean values are listed over 25000 snapshots with 0.2 ps intervals. The standard free energy (G^0_{fi} and G^0_s) and standard free energy gap (ΔG^0_{fi} and ΔG^0_s) are listed in Table 2.
[b] GT was derived from Eq. (20).
[c] GTRAM was derived from Eq. (21).
[d] The rate was derived from Eqs. (1) and (4) for the fast and slow component, respectively.

[30] (0.63 nm) and FDs [33] (0.67 nm). The ET processes in both the fast and slow components should be adiabatic, because the R_c values in P2O were much shorter than these critical ET distances.

The static dielectric constants inside the protein of the fast and slow components (ε^f_0 and ε^s_0) were similar to each other (11.4 and 10.8), but much higher than those in the WT FBP (5.8) [30] and FD (3.8) [33]. The static dielectric constants near the Trp168 donor and Iso acceptor were 9.78 and 5.76 in the fast and slow components, respectively, which were considerably higher than those of FBP (2.2) [30] and FD (2.3) [33]. This suggests that the dielectric constants both inside the protein and near the donor and acceptor were higher in P2O than those in FBP and FD.

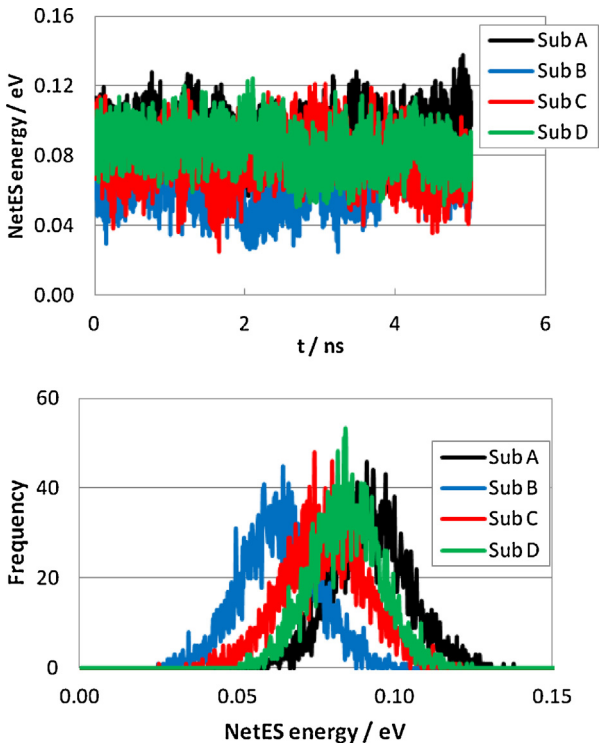

Fig. 5. The (upper panel) time evolution and (lower panel) distribution of the NetES energy in the subunits of the P2O tetramer.
The NetES was derived from Eqs. (7) and (8).

3.5. ET rate from Trp168 to Iso*

Time-evolutions of the logarithmic ET rates are shown in Fig. S1 (SI), whilst the distributions of the logarithmic ET rates from Trp160 to Iso* are shown in Fig. 4. The slow component with a 358 ps lifetime was assigned to be Sub A and was emission-wavelength independent. The fast components were assigned as Sub B, Sub C and Sub D with emission-wavelength dependent fluorescent lifetimes (Table S2, SI). From this assignment of the slow and fast components, the concentration ratio of the fast/slow components should be 3. The concentration ratio relates to α_1/α_2, but this had a much higher mean value of 8.6 (Table S2, SI), [12] which suggests an additional ultrafast emission component is contained in the fast decay [12,38] that contributes to the higher α_1/α_2 value. In the present work we adopted a simpler model with two-emission components expressed by τ_1 and τ_2. The maximum distribution of the logarithmic ET rates was around −5.8 in Sub A, where the ET rate was expressed in ps^{-1} (Fig. 4), whilst that for the fast component was similar between Sub C and Sub D at all emission wavelengths but lower than that for Sub B at all emission wavelengths except for 480 nm. The derived mean values of the ET rates and logarithmic ET rates are listed in Table 3. The ET rate of the slow component was 0.00296 ps^{-1}, with an inversion value of 338 ps that was close to the experimental lifetime of 358 ps. The ET rates of Sub B were always the fastest among the three fast subunits (components) at all emission wavelengths. The inverse values of the average ET rates over the three fast subunits (11.0, 9.04, 9.30, 14.4 and 17.5 ps^{-1} at 580, 555, 530, 500 and 480 nm, respectively) were 0.091, 0.111, 0.108, 0.069 and 0.057 ps, respectively, which compared well with the experimental lifetimes of 0.092, 0.113, 0.11, 0.07 and 0.057 ps at 580, 555, 530, 500 and 480 nm, respectively. Thus, the agreement between the calculated and observed lifetimes was excellent at all emission wavelengths.

3.6. Physical quantities independent of the emission wavelength

Among several physical quantities related to the ET rate, the NetES energy (E^{ic}_{Net}), solvent reorganization energy (λ^{ic}_S), and ESDA ($-e^2/\varepsilon^c_{DA}R_i$), are emission-wavelength independent. The time-evolution and distribution of the NetES energy, derived from Eq. (8), between the photo-products and ionic species inside the protein had a slightly lower peak in Sub B than those in the other fast subunits (Fig. 5). The derived mean values of the NetES energy

Table 4
Mean physical quantities independent of the emission wavelength.[a]

Quantity	Sub A	Sub B	Sub C	Sub D
λ_S^{ic}[b] (eV)	1.62	1.84	1.87	1.86
$-e^2/\varepsilon_{DA}^c R_i$[c] (eV)	−0.335	−0.247	−0.238	−0.241
E_{Net}^{ic}[d] (eV)	0.0920	0.0634	0.0777	0.0845
E_{Net}^{i}in vacuum[e] (eV) (single subunit)	0.406	0.309	0.250	0.442
E_{Net}^{i}in vacuum[f] (eV) (all subunits)	0.991	0.725	0.886	0.962
EC[g] (ps^{-1})	535	959	535	535
ln EC	6.28	6.87	6.28	6.28
SQRT[h]	0.0331	0.0354	0.0329	0.0330
ln SQRT	−3.41	−3.34	−3.41	−3.41

[a] Mean physical quantities were obtained over 25000 snapshots with 0.2 ps intervals.
[b] Solvent reorganization energy given by Eqs. (2) and (5).
[c] ES energy between Iso anion and Trp168 cation.
[d] NetES energy given by Eq. (8).
[e] NetES energy with $\varepsilon_0^c = 1$ (vacuum) within single subunit.
[f] NetES energy with $\varepsilon_0^c = 1$ (vacuum) over the entire protein.
[g] Electronic coupling term given by $\frac{\nu_0^c}{1+\exp\{\beta^c(R_i-R_0^c)\}}$.
[h] Root of square term, $\sqrt{\frac{k_BT}{4\pi\lambda_S^{ic}}}$.

over 25000 snapshots with 0.2 ps time intervals are listed in Table 4. The mean values of E_{Net}^{i} ranged from 0.092 eV in Sub A down to 0.0634 eV in Sub B. In any of the subunits, however, the E_{Net}^{ic} values were negligibly low compared to the other energies, which is ascribed to the fairly high static dielectric constants inside the protein ($\varepsilon_0^f = 11.4$; $\varepsilon_0^s = 10.8$; Table 3).

The time-evolutions and distributions of λ_S^{ic} are shown in Fig. 6, where the λ_S^{ic} values in Sub A were markedly lower than those in the three fast subunits. The mean values of λ_S^{ic} (Table 4) ranged from 1.62 eV in Sub A (slow fluorescent lifetime) to 1.84–1.87 eV in Sub B, Sub C and Sub D (fast fluorescent lifetime). The time-evolutions and distributions of ESDA ($-e^2/\varepsilon_{DA}^c R_i$) are shown in

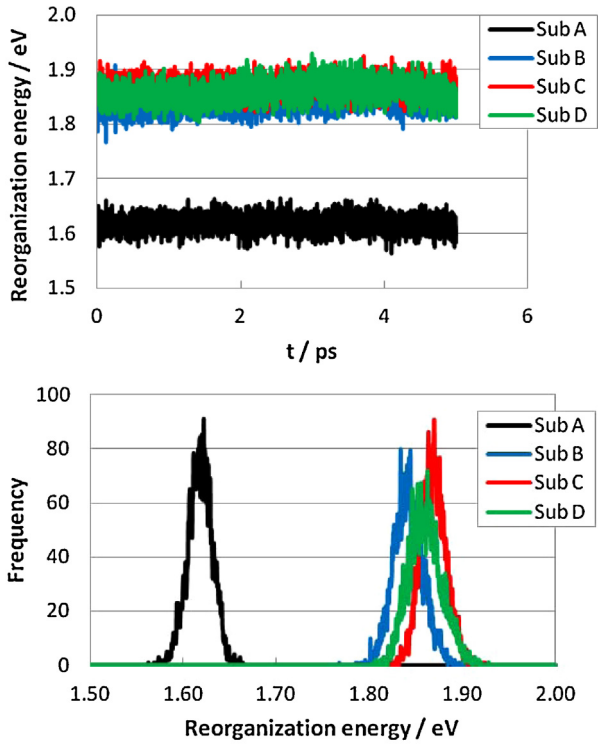

Fig. 6. The (upper panel) time-evolution and (lower panel) distribution of the solvent reorganization energy in the subunits of the P2O tetramer.
The reorganization energy was derived from Eqs. (2) and (5).

Fig. 7, with the derived mean values of ESDA listed in Table 4. The ESDA was markedly lower in Sub A, compared to those in the three fast subunits, with mean values of −0.335 eV in Sub A and −0.238 to −0.247 eV in the three fast subunits.

The logarithmic ET rate may be decomposed into three terms, as in Eq. (17), each defined as in Eqs. (18)–(21).

$$\ln k_i^c = \ln EC + \ln SQRT + GTRAM \tag{17}$$

$$\ln EC = \ln \frac{\nu_0^c}{1+\exp\{\beta^c(R_i - R_0^c)\}} \tag{18}$$

$$\ln SQRT = \ln \sqrt{\frac{k_BT}{4\pi\lambda_S^{ic}}} \tag{19}$$

$$GT = \Delta G_c^0 - e^2/\varepsilon_{DA}^c R_i + \lambda_S^{ic} + E_{Net}^{ic} \tag{20}$$

$$GTRAM = -\frac{\{GT\}^2}{4\lambda_S^{ic} k_BT} \tag{21}$$

In Eqs. (16)–(20), the suffix c denotes f (fast component) or s (slow component), EC is an electronic coupling term. GT is total free energy gap and GTRAM is an exponential term, and all are dependent on the emission wavelength j. The terms k_{ij}^f and k_i^s for the fast and slow components are given by Eqs. (1) and (4), respectively. The quantities EC (ln EC) and SQRT (ln SQRT) are emission-wavelength independent.

The time-evolution of ln EC revealed that the ln EC values were almost constant with time (Fig. 8), which is ascribed to the large R_0^f and R_0^s values (Table 3) that were much longer than R_c. Accordingly, the ET processes are adiabatic in both the slow and fast subunits. The mean values of EC were 959 ps^{-1} in Sub A and 535 ps^{-1} in Sub B, Sub C and Sub D (Table 4). The values of SQRT were 0.0354 ps^{-1} in Sub A and 0.0329–0.0331 ps^{-1} in Sub B, Sub C and Sub D.

3.7. Physical quantities dependent on the emission wavelength

The standard free energy related to the electron affinity of Iso* (G_{fi}^0 and G_s^0) and its free energy gap (ΔG_{fi}^0 and ΔG_s^0) are emission-wavelength dependent (Table 2). The value of G_s^0 was 7.33 eV, which was ca. 1 eV lower than those of G_{fi}^0. Likewise, GT and GTRAM were also emission-wavelength dependent with mean GT values of 0.16–0.37 eV in the fast subunits at 580–500 nm and −0.03 to 0.02 eV at 480 nm (Table 3). In the slow component (Sub A), the values of GT was 1.24 eV. The mean GTRAM value of the three subunits of the fast component was −0.47 at 580 nm, increasing to −0.68 and −0.65 at 555 and 530 nm, −0.65 at 530 nm, respectively, and then falling markedly to −0.21 and −0.0066 at 500 and 480 nm, respectively, compared to -9.4 in the Sub A. Absolute value of GTRAM was markedly higher in the slow component (Sub A) than those in the fast component subunits.

3.8. Dutton rule

The dependence of the logarithmic ET rate on the donor–acceptor distance (Dutton rule) [25] is shown in Fig. 9 for Sub A (slow component) and Sub C (representative fast component subunit). In all subunits, including Sub A, the logarithmic rates were well approximated by linear functions (Y (ln Rate) = aX (R_c) + b) at 580 nm, 555 nm and 530 nm (fast subunits). The slope

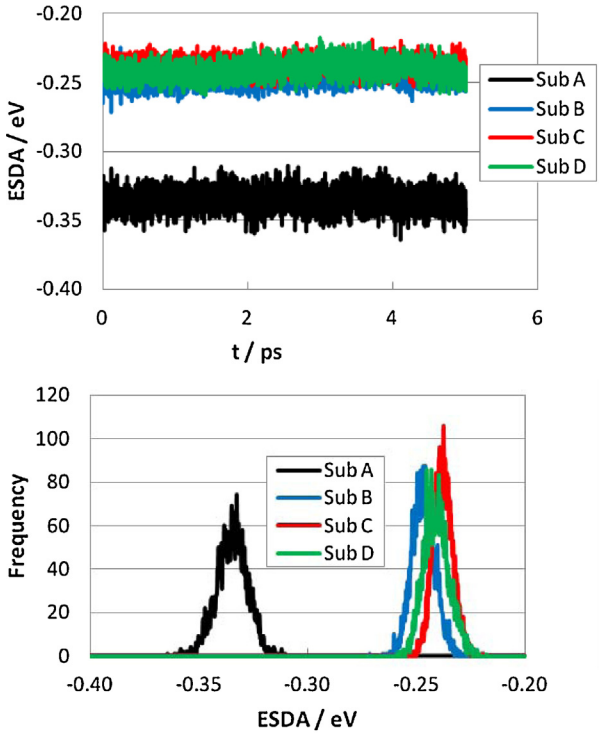

Fig. 7. The (upper panel) time-evolution and (lower panel) distribution of the ESDA energy in the subunits of the P2O tetramer.

(a) was −18.3 in Sub A, which was much steeper than those (−4.5 to −6) in the fast subunits at 580–530 nm. At 500 nm and 480 nm, the logarithmic rates were well approximated by a parabolic function ($Y = aX^2 + bX + c$), where the derived coefficients, a, b and c are listed in Table 5.

The relationships between GTRAM and R_c are shown in Fig. 10 and Table 5 for Sub A and Sub C, where the values of GTRAM were well approximated with linear functions of R_c at 580, 555 and 530 nm. However, at 500 and 480 nm the relationship was slightly and clearly parabolic, respectively. The approximated functions were similar to those of the ln Rate *vs.* R_c correlations. The slope of the linear function in Sub A was −18.0 in the GTRAM *vs.* R_c plot (Table 5), which was similar to that (−18.3) of the ln Rate *vs.* R_c, whilst for Sub B it was −5.23, −5.51 and −5.12 at 580, 555 and 530 nm, respectively, which compared well to those in the ln Rate *vs.* R_c plots of −5.23 nm, −5.51 and −5.12, respectively. Likewise for Sub C it was −5.7, −5.95 and −5.6 at 530 nm, respectively, in the GTRAM *vs.* R_c plots compared to −5.11, −5.95 and −5.85, respectively, in the Rate *vs.* R_c plots, and for Sub D was −4.36, −5.12 and −5.02, respectively, compared to −4.61, −5.73 nm and −3.48, respectively. It was, therefore, concluded that the Dutton rule in these adiabatic ET processes are determined by GTRAM.

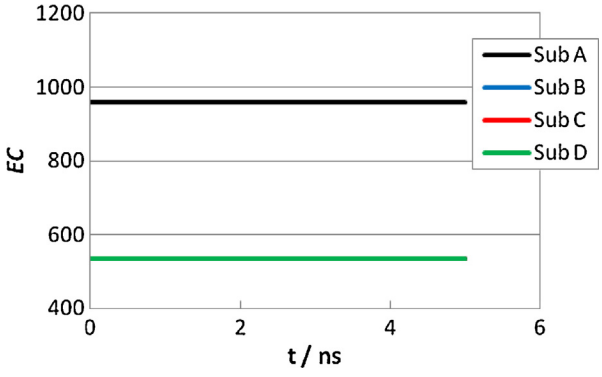

Fig. 8. Time-evolution of EC for the different subunits of the P2O tetramer. EC was derived from Eq. (18) and is expressed in ps^{-1}. The time-evolution of EC for subunit B and C are overlapping.

3.9. Numerical elucidation why ET rate is 4000-fold slower in the slow component subunit than that in the fast component subunits.

The most remarkable difference between Sub A and the other subunits was in the GTRAM, where the GTRAM value was −9.4 in Sub A but some 15.7- to 1,343-fold lower (−0.6 to −0.007) in the fast subunits (Table 3). This is likely to then be the main reason why the ET rate in Sub A is much longer than those in the fast subunits. That the absolute value of GTRAM was markedly larger in Sub A than in the three fast subunits was because the GT value of Sub A (1.24 eV) was much larger than those in the fast subunits (0–0.4 eV). From Eq. (20), GT is seen to consist of the four terms, ΔG_c^0, $-e^2/\varepsilon_{DA}^c R_i$, λ_S^{ic}, and E_{Net}^{ic}. The value of ΔG_c^0 was −0.13 eV in Sub A, but over 10-fold higher (around −1.4 eV) in the fast subunits (Table 2). In contrast the other components did not vary as dramatically. The value of $-e^2/\varepsilon_{DA}^c R_i$ was −0.34 eV in Sub A, compared to slightly less at around −0.24 eV in the fast subunits, λ_S^{ic} was 1.6 in Sub A and around 1.9 eV in the fast subunits, and E_{Net}^{ic} was 0.09 eV in Sub A and around 0.075 eV in the fast subunits. Thus, the large difference in the GT value between Sub A and the other subunits was ascribed principally to the difference in the ΔG_c^0 values, and so is likely to be the main reason for the large difference in the fluorescence lifetime between the slow (358 ps) and fast (mean 88 fs) components.

3.10. High polarity around Iso

The polarity near the donor and Iso determined by ε_{DA}^s (5.76) for the slow subunit and by ε_{DA}^f (9.78) for the fast subunits, was higher in the fast component subunits than in the slow one (Sub A). The relatively high polarity near Iso is explained by the presence of many water molecules near Iso in P2O. The radial distribution functions (RDF) of water molecules near Iso considered to be the mean number of water molecules over the MDS snapshots, is shown in Fig. 11. The total number of water molecules (sums over all Iso heteroatoms) was approximately 10 in Sub A, 16 in Sub B, 14 in Sub C and 12 in Sub D, which suggests that a fair number of water molecules were present near Iso. P2O is an enzyme, so that a space pocket exists near Iso for its substrate binding. The RDF near Trp168 is shown in Fig. S2 (SI), where water molecules exist at quite distant places longer than 0.6 nm from the indole ring atoms.

4. Discussion

Extraordinary heterogeneity in the fluorescence lifetime in P2O was elucidated with MDS coordinates of atoms in P2O and the KM ET rate. It was assigned that the slow component (τ_s = 358 ps) is Sub A, and the fast component (mean τ_f = 88 fs) is Sub B, Sub C and Sub D. The emission-wavelength dependent lifetimes of the fast component were explained by introducing the emission-wavelength dependent free energy related to the electron affinity of Iso*. Agreements were all excellent between the calculated and observed fluorescence decays of both the slow and fast components. The ET processes from Trp168 to Iso were adiabatic in both the slow and fast components. The main factor for the great difference in the lifetimes between the slow and fast components was the standard free energy gap, which was 0.13 eV in the slow component and −1.4 eV in the fast component.

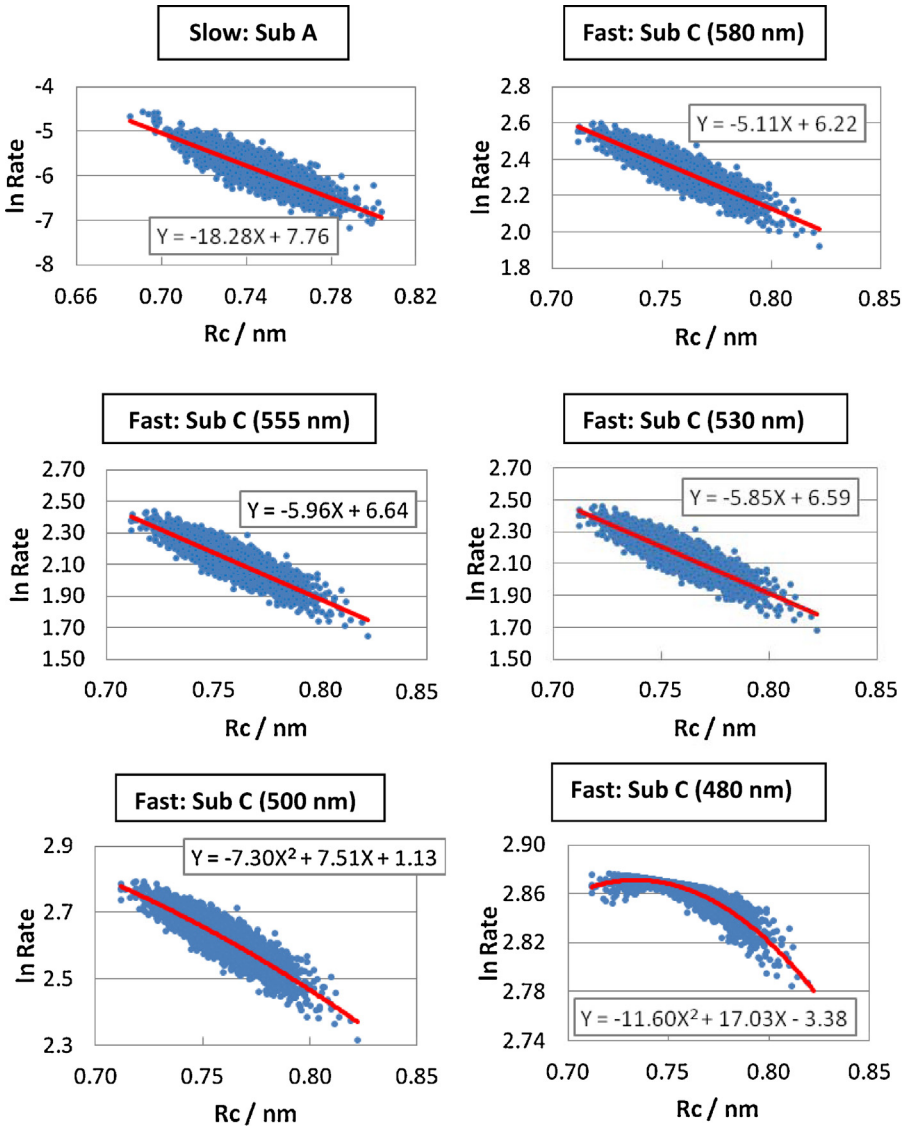

Fig. 9. The Dutton law in the P2O tetramer.
The slow component (Sub A) and the fast component (Sub C as a representative example) at different emission wavelengths. The slow component of Sub A does not show any emission-wavelength dependence. Inserts indicate approximation functions of logarithmic ET rate with R_c. The coefficients of the functions are listed in Table 5.

Table 5
Coefficients in approximate functions of ln Rate *vs.* R_c and of GTRAM *vs.* R_c.[a]

Subunit	Wavelength (nm)	Coefficient					
		ln Rate *vs.* R_c			GTRAM *vs.* R_c		
		a	b	c	a	b	c
Sub A	–	−18.28	7.76	–	−18	4.04	–
Sub B	580	−4.61	5.87	–	−5.23	3.26	–
	555	−5.51	6.33	–	−5.51	6.33	–
	530	−5.4	6.28	–	−5.12	3.21	–
	500	−10.5	12.4	−0.723	−10.9	13.3	−4.03
	480	−13	19.2	−4.24	−13.4	20.13	−7.55
Sub C	580	−5.11	6.22	–	−5.7	3.58	–
	555	−5.95	6.64	–	−5.95	6.64	–
	530	−5.85	6.59	–	−5.6	3.53	–
	500	−7.3	7.51	1.13	−7.68	8.34	−2.15
	480	−11.6	17	−3.38	−11.99	17.87	−6.66
Sub D	580	−4.61	5.81	–	−4.36	2.75	–
	555	−5.37	6.17	–	−5.12	3.11	–
	530	−5.28	6.13	–	−5.02	3.07	–
	500	−3.48	2	3.09	−3.88	2.86	−0.194
	480	−9.37	13.6	−2.05	−9.77	14.44	−5.34

[a] Linear functions are expressed by Y = aX + b, and parabolic functions by Y = aX2 + bX + c.

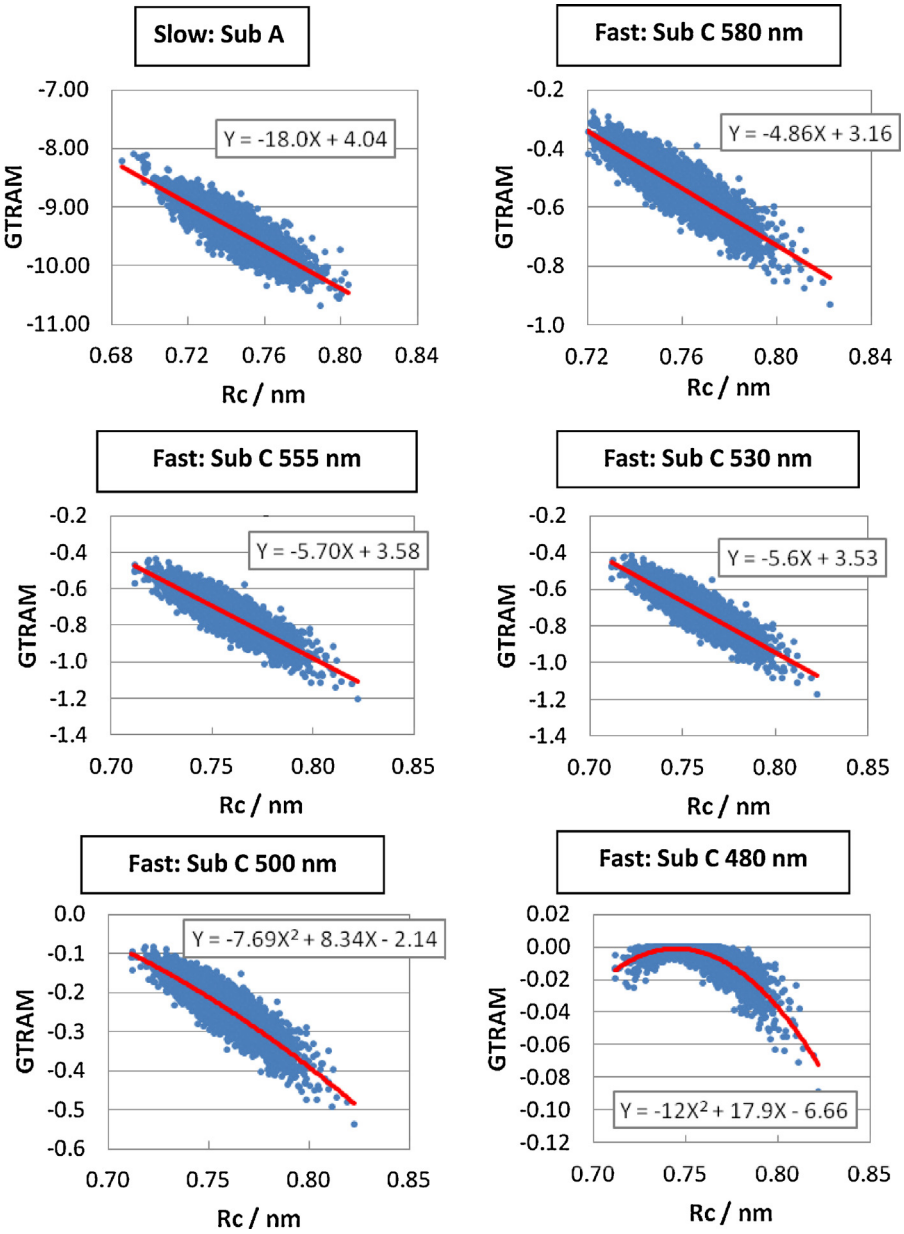

Fig. 10. Relationship between GTRAM and R_c in Sub A and Sub C.
GTRAM was derived from Eq. (21). Insert denotes the approximate function, Y (GTRAM) *vs.* X (R_c).

The polarity near the donor and Iso was higher in the fast subunits than in the slow subunit, as determined by the ε^s_{DA} and ε^f_{DA} values of 5.76 and 9.78 for the slow and fast subunits, respectively. This is in accordance with the observed transient fluorescence spectra in the WT P2O, with an emission peak at around 510 and 540 nm in the slow and fast components, respectively [12]. The relatively high polarity around Iso is likely to reflect the presence of from 10 (Sub A) to 16 (Sub B) water molecules near Iso in each subunit, potentially around the space pocket (P2O substrate binding site) near Iso since the water molecules were more than 0.6 nm distance from the indole ring.

The emission-wavelength of the slow component is quite short despite the fact that the ε^s_{DA} (5.76) was higher than the ε_{DA} (2.25) in the FD from *H. pylori*, which displays the fluorescence peak at 524 nm [33]. However, the relationship between the values of ε_{DA} and the peak wavelength of the fluorescence spectrum may not be straightforward. Generally, a maximum fluorescence wavelength of flavin depends on both the polarity around flavin and H-bond formation between heteroatoms of Iso and nearby amino acids. The transition energy of Iso in the ground state is strongly influenced by H-bond formation between a heteroatom in Iso and H-bond partner for it [39]. All of the heteroatoms in Iso formed H-bonds with nearby amino acids (Table S3, SI), in which Iso is in the ground electronic state. The effect of H-bond formation on the fluorescence wavelength of Iso should be examined in the excited state by molecular orbital theory, as the effect of H-bonds on the absorption spectrum examined by Nishimoto et al. [39].

With respect to the Dutton rule in P2O, the approximate functions of the ln Rate *vs.* R_c were linear in the slow component and the fast component at 580 nm, 555 nm and 530 nm, where the lifetimes were relatively long. The EC terms did not depend on R_c in P2O, because the ET processes were adiabatic. A linear relationship was found in GTRAM terms, which shows that the exponential terms in the KM rate approximately display the linear relation.

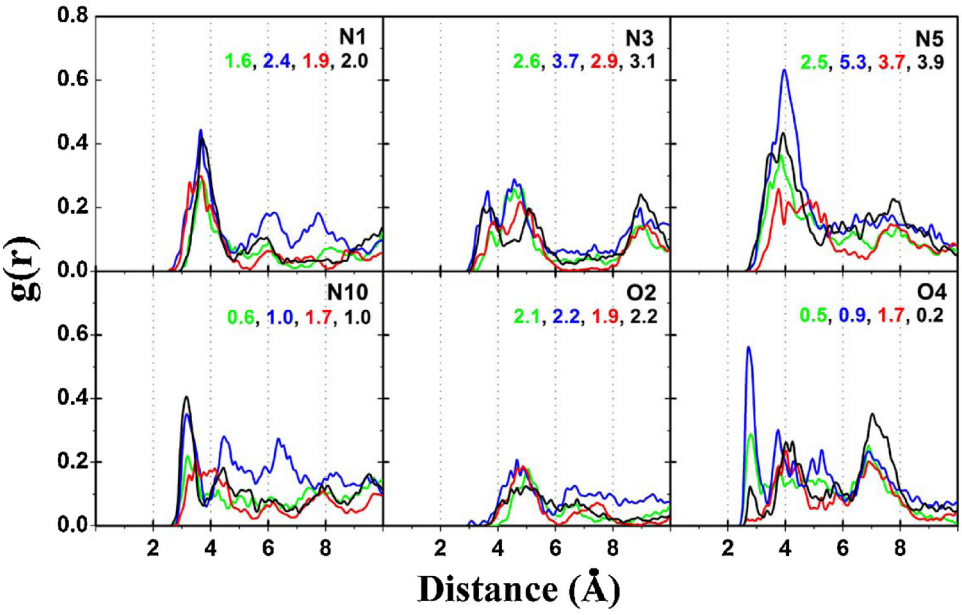

Fig. 11. The radial distribution function (g(r)) of water molecules near Iso in the P2O subunits.
Atom notations of N1, N3, N5, N10, O2 and O4 are given in Chart 1. The integrated number of water molecules are indicated in green for subunit A, in blue for subunit B, in red for subunit C and in black for subunit D.

The approximate functions in the fast component at 500 nm and 480 nm were parabolic, where the lifetimes were shorter. It was also found that Dutton rule becomes parabolic when the lifetime is ultrashort [40–42]. It was pointed out that ETRAM term plays important role on Dutton rule in these ultrafast ET systems. At shorter distances than one of peak ln Rate, the ET rate becomes slower despite that the interaction between the donor and acceptor becomes stronger. This does not seem to be reasonable, so that Marcus theory and also KM rate may be not valid in this region of the distances.

Acknowledgments

This work was supported by The Ratchadaphiseksomphot Endowment Fund of Chulalongkorn University. K. L. would like to acknowledge the postdoctoral fellowship of Chulalongkorn University. We would like to thank The National e-Science Infrastructure Consortium for providing computing resources.

Appendix A. Supplementary data

Supplementary data associated with this article can be found, in the online version, at http://dx.doi.org/10.1016/j.jphotochem.2015.03.016

References

[1] G. Daniel, J. Volc, E. Kubatova, Pyranose oxidase, a major source of H_2O_2 during wood degradation by *Phanerochaete* chrysosporium, *Trametes* versicolor, and *Oudemansiella* mucida, Appl. Environ. Microbiol. 60 (1994) 2524–2532.
[2] R. ten Have, P.J.M. Teunissen, Oxidative mechanisms involved in lignin degradation by white-rot fungi, Chem. Rev. 101 (2001) 3397–3414.
[3] C. Leitner, J. Volc, D. Haltrich, Purification and characterization of pyranose oxidase from the white rot fungus trametes multicolor, Appl. Environ. Microbiol. 67 (2001) 3636–3644.
[4] P. Halada, C. Leitner, P. Sedmera, D. Haltrich, J. Volc, Identification of the covalent flavin adenine dinucleotide-binding region in pyranose 2-oxidase from *Trametes* multicolor, Anal. Biochem. 314 (2003) 235–242.
[5] B. Martin Hallberg, C. Leitner, D. Haltrich, C. Divne, Crystal structure of the 270 kDa homotetrameric lignin-degrading enzyme pyranose 2-oxidase, J. Mol. Biol. 341 (2004) 781–796.
[6] M. Kujawa, H. Ebner, C. Leitner, B.M. Hallberg, M. Prongjit, J. Sucharitakul, R. Ludwig, U. Rudsander, C. Peterbauer, P. Chaiyen, D. Haltrich, C. Divne, Structural basis for substrate binding and regioselective oxidation of monosaccharides at C3 by pyranose 2-oxidase, J. Biol. Chem. 281 (2006) 35104–35115.
[7] T.-C. Tan, W. Pitsawong, T. Wongnate, O. Spadiut, D. Haltrich, P. Chaiyen, C. Divne, H-bonding and positive charge at the N(5)/O(4) locus are critical for covalent flavin attachment in *Trametes* pyranose 2-oxidase, J. Mol. Biol. 402 (2010) 578–594.
[8] J. Sucharitakul, M. Prongjit, D. Haltrich, P. Chaiyen, Detection of a C4a-hydroperoxyflavin intermediate in the reaction of a flavoprotein oxidase, Biochemistry 47 (2008) 8485–8490.
[9] M. Prongjit, J. Sucharitakul, T. Wongnate, D. Haltrich, P. Chaiyen, Kinetic mechanism of pyranose 2-oxidase from *Trametes* multicolor, Biochemistry 48 (2009) 4170–4180.
[10] J. Sucharitakul, T. Wongnate, P. Chaiyen, Kinetic isotope effects on the noncovalent flavin mutant protein of pyranose 2-oxidase reveal insights into the flavin reduction mechanism, Biochemistry 49 (2010) 3753–3765.
[11] W. Pitsawong, J. Sucharitakul, M. Prongjit, T.-C. Tan, O. Spadiut, D. Haltrich, C. Divne, P. Chaiyen, A conserved active-site threonine is important for both sugar and flavin oxidations of pyranose 2-oxidase, J. Biol. Chem. 285 (2010) 9697–9705.
[12] H. Chosrowjan, S. Taniguchi, T. Wongnate, J. Sucharitakul, P. Chaiyen, F. Tanaka, Conformational heterogeneity in pyranose 2-oxidase from Trametes multicolor revealed by ultrafast fluorescence dynamics, J. Photochem. Photobiol. A: Chem. 234 (2012) 44–48.
[13] S. Taniguchi, H. Chosrowjan, F. Tanaka, T. Nakanishi, S. Sato, Y. Haruyama, M. Kitamura, A key factor for ultrafast rates of photoinduced electron transfer among five flavin mononucleotide binding proteins: effect of negative, positive, and neutral charges at residue 13 on the rate, Bull. Chem. Soc. Jpn. 86 (2013) 339–350.
[14] T. Kakitani, N. Mataga, New energy gap laws for the charge separation process in the fluorescence quenching reaction and the charge recombination process of ion pairs produced in polar solvents, J. Phys. Chem. 89 (1985) 8–10.
[15] A. Yoshimori, T. Kakitani, Y. Enomoto, N. Mataga, Shapes of the electron-transfer rate vs energy gap relations in polar solutions, J. Phys. Chem. 93 (1989) 8316–8323.
[16] N. Matsuda, T. Kakitani, T. Denda, N. Mataga, Examination of the viability of the Collins-Kimball model and numerical calculation of the time-dependent energy gap law of photoinduced charge separation in polar solution, J. Chem. Phys. 190 (1995) 83–95.
[17] N. Mataga, H. Chosrowjan, S. Taniguchi, Ultrafast charge transfer in excited electronic states and investigations into fundamental problems of exciplex chemistry: our early studies and recent developments, J. Photochem. Photobiol. C: Photochem. Rev. 6 (2005) 37–79.
[18] K. Lugsanangarm, S. Kokpol, A. Nueangaudom, S. Pianwanit, N. Nunthaboot, F. Tanaka, Structural heterogeneity among four subunits in pyranose 2-oxidase: a molecular dynamics simulation study, J. Theor. Comput. Chem. 13 (2014) 1440010.
[19] D.A. Case, T.A., Darden, T.E., Cheatham III, C.L. Simmerling, J. Wang, R.E. Duke, R. Luo, M. Crowley, R.C. Walker, W. Zhang, K.M. Merz, B. Wang, S. Hayik, A. Roitberg, G. Seabra, I. Kolossváry, K.F. Wong, F. Paesani, J. Vanicek, X. Wu, S.R. Brozell, T. Steinbrecher, H. Gohlke, L. Yang, C. Tan J. Mongan, V. Hornak, G. Cui,

H.D. Mathews, M.G. Seetin, C. Sagui, V. Babin, P.A. Kollman, AMBER10, University of California, San Francisco, 2008.
[20] K. Lugsanangarm, S. Pianwanit, S. Kokpol, N. Nunthaboot, H. Chosrowjan, S. Taniguchi, F. Tanaka, Theoretical analyses of photoinduced electron transfer in medium chain acyl-CoA dehydrogenase: electron transfer in the normal region, J. Photochem. Photobiol. A: Chem. 224 (2011) 80–90.
[21] J.-P. Ryckaert, G. Ciccotti, H.J.C. Berendsen, Numerical integration of the cartesian equations of motion of a system with constraints: molecular dynamics of *n*-alkanes, J. Comput. Phys. 23 (1977) 327–341.
[22] U. Essmann, L. Perera, M. Berkowitz, T. Darden, H. Lee, L. Pedersen, A smooth particle mesh Ewald method, J. Chem. Phys. 103 (1995) 8577–8593.
[23] R.J. Marcus, The theory of oxidation-reduction reactions involving electron transfer I, J. Chem. Phys. 24 (1956) 969–978.
[24] R.A. Marcus, Chemical and electrochemical electron-transfer theory, Annu. Rev. Phys. Chem. 15 (1964) 155–196.
[25] C.C. Moser, J.M. Keske, K. Warncke, R.S. Farid, P.L. Dutton, Nature of biological electron transfer, Nature 355 (1992) 796–802.
[26] H. Chosrowjan, S. Taniguchi, N. Mataga, T. Nakanishi, Y. Haruyama, S. Sato, M. Kitamura, F. Tanaka, Effects of the disappearance of one charge on ultrafast fluorescence dynamics of the FMN binding protein, J. Phys. Chem. B 114 (2010) 6175–6182.
[27] A. Nueangaudom, K. Lugsanangarm, S. Pianwanit, S. Kokpol, N. Nunthaboot, F. Tanaka, Structural basis for the temperature-induced transition of d-amino acid oxidase from pig kidney revealed by molecular dynamic simulation and photo-induced electron transfer, Phys. Chem. Chem. Phys. 14 (2012) 2567–2578.
[28] A. Nueangaudom, K. Lugsanangarm, S. Pianwanit, S. Kokpol, N. Nunthaboot, F. Tanaka, The mechanism of photoinduced electron transfer in the d-amino acid oxidase–benzoate complex from pig kidney: electron transfer in the inverted region, J. Photochem. Photobiol. A: Chem. 250 (2012) 6–17.
[29] N. Nunthaboot, F. Tanaka, S. Kokpol, H. Chosrowjan, S. Taniguchi, N. Mataga, Simultaneous analysis of ultrafast fluorescence decays of FMN binding protein and its mutated proteins by molecular dynamic simulation and electron transfer theory, J. Phys. Chem. B 112 (2008) 13121–13127.
[30] N. Nunthaboot, S. Pianwanit, S. Kokpol, F. Tanaka, Simultaneous analyses of photoinduced electron transfer in the wild type and four single substitution isomers of the FMN binding protein from *Desulfovibrio* vulgaris, Miyazaki F, Phys. Chem. Chem. Phys. 13 (2011) 6085–6097.
[31] N. Nunthaboot, N. Kido, F. Tanaka, K. Lugsanangarm, A. Nueangaudom, S. Pianwanit, S. Kokpol, Relationship between rate of photoinduced electron transfer and hydrogen bonding chain of tyrosine–glutamine–flavin in flavin photoreceptors: global analyses among four TePixDs and three AppAs, J. Photochem. Photobiol. A: Chem. 252 (2013) 14–24.
[32] K. Lugsanangarm, S. Pianwanit, S. Kokpol, F. Tanaka, H. Chosrowjan, S. Taniguchi, N. Mataga, Photoinduced electron transfer in wild type and mutated flavodoxin from *Desulfovibrio* vulgaris, strain Miyazaki F.: energy gap law, J. Photochem. Photobiol. A: Chem. 219 (2011) 32–41.
[33] K. Lugsanangarm, S. Pianwanit, A. Nueangaudom, S. Kokpol, F. Tanaka, N. Nunthaboot, K. Ogino, R. Takagi, T. Nakanishi, M. Kitamura, S. Taniguchi, H. Chosrowjan, Mechanism of photoinduced electron transfer from tyrosine to the excited flavin in the flavodoxin from *Helicobacter* pylori. A comparative study with the flavodoxin and flavin mononucleotide binding protein from *Desulfovibrio* vulgaris (Miyazaki F), J. Photochem. Photobiol. A: Chem. 268 (2013) 58–66.
[34] V. Vorsa, T. Kono, K.F. Willey, N. Winograd, Femtosecond photoionization of ion beam desorbed aliphatic and aromatic amino acids: fragmentation via α-cleavage reactions, J. Phys. Chem. B 103 (1999) 7889–7895.
[35] M. Ohe, H. Matsuo, F. Sakyama, N. Kozo, Determination of pK_a's of individual histidine residues in pancreatic ribonuclease by hydrogen–tritium exchange, J. Biochem. (Tokyo) 75 (1974) 1179–1200.
[36] J.L. Markley, Correlation proton magnetic resonance studies at 250MHz of bovine pancreatic ribonuclease. I. Reinvestigation of the histidine peak assignments, Biochemistry 14 (1975) 3546–3554.
[37] M. Miyagi, T. Nakazawa, Determination of pK_a values of individual histidine residues in proteins using mass spectrometry, J. Anal. Chem. 80 (2008) 6481–6487.
[38] S. Taniguchi, H. Chosrowjan, T. Wongnate, J. Sucharitakul, P. Chaiyen, F. Tanaka, Ultrafast fluorescence dynamics of flavin adenine dinucleotide in pyranose 2-oxidases variants and their complexes with acetate: conformational heterogeneity with different dielectric constants, J. Photochem. Photobiol. A: Chem. 245 (2012) 33–42.
[39] K. Nishimoto, Y. Watanabe, K. Yagi, Hydrogen bonding of flavoprotein. I. Effect of hydrogen bonding on electronic spectra of flavoprotein, Biochim. Biophys. Acta. Enzymol. 526 (1978) 34–41.
[40] N. Nunthaboot, K. Lugsanangarm, S. Pianwanit, S. Kokpol, F. Tanaka, S. Taniguchi, H. Chosrowjan, T. Nakanishi, M. Kitamura, Bell-shaped dependence of the rate of ultrafast photoinduced electron transfer from aromatic amino acids to the excited flavin on the donor–acceptor distance in FMN binding proteins, J. Comput. Theor. Chem. 1030 (2014) 9–16.
[41] F. Tanaka, H. Chosrowjan, S. Taniguchi, N. Mataga, K. Sato, Y. Nishina, K. Shiga, Donor–acceptor distance-dependence of photoinduced electron-transfer rate in flavoproteins, J. Phys. Chem. B 111 (2007) 5694–5699.
[42] F. Tanaka, R. Rujkorakarn, H. Chosrowjan, S. Taniguchi, N. Mataga, Analyses of donor–acceptor distance-dependent rates of photo-induced electron transfer in flavoproteins with three kinds of electron transfer theories, Chem. Phys. 348 (2008) 237–241.